Jour. Fac. Sci., Hokkaido Univ., Ser. VII (Geophysics), Vol. 11, No. 3, 633-655, 1999.

Systems of Multiply Connected Nonlinear Oscillators and Their Application to Seismic Phenomena

Itaru Maeda and Masatoshi Yokomori

Division of Earth and Planetary Science, (Geophysics)
Graduate School of Science, Hokkaido University,
Sapporo 060-0810, Japan

(Received November 30, 1998)

Abstract

We constructed and analyzed systems consisting of nonlinear oscillators and applied them to seismic phenomena. The nonlinear oscillator originally invented by Rayleigh more than a hundred years ago is a mass placed on a moving belt and exerted forces through nonlinear friction and a linear spring. The nonlinearity characterizes the oscillator which we call Rayleigh oscillator. We first made elementary analyses on a system of a single oscillator and determined the Hopf bifurcation point. Next, we constructed a coupled Rayleigh oscillators and analyzed it mainly numerically. The bifurcation diagram shows clearly famous period doubling sequences at several ranges of the parameter presenting driving velocity of the belt. This means that the system makes chaotic motions. This two oscillator system has so called inverse power law nature which is called Gutenberg-Richiter relation in seismology. We extended it to a system of multiply connected (10 to 30) oscillators. We showed numerically that the system's behavior was so complex as being stochastic and actually be ergodic for long term behavior, though the ruling differential equations are deterministic. We scaled magnitude (log amplitude) and time of the model system to be able to compare with natural seismic phenomena. We constructed energy release curves for real seismic data observed over 35 years in several regions and for model events over extremely long time period. Examination of a correlation between these curves shows that the system of multiply connected Rayleigh oscillators can be a predictor of seismic activities.

1. Introduction

Although it has been a long time since Brace and Byerlee (1966) announced that seismic events were considered to be stick-slip motions, the history of the idea of stick-slip was very much older than the discovery by Brace et al. Rayleigh (1894) analyzed and formulated, for example, vibration of a violin string excited by bowing as a stick-slip motion. We try to combine Rayleigh's

formulation with Brace and Byerlee's idea to simulate seismic activities, one of which is expressed by Gutenberg-Richiter relation (see for example, Utsu, 1977).

Almost all researches for the simulation are the descendants of the work by Burridge and Knopoff (1967). These models consist, basically, of multiple blocks connected by springs and sliders with each other and with a driving source. These springs and sliders are linear or non-linear. Because the stick and slip conditions expressed by so-called constitutive equations are artificially and numerically given in these researches, any analytical evaluation of these models is out of the question.

Rayleigh's study is motivated by the following question; why can a violin bow moving in one direction sustain vibration of the string? The bow exerts forces to the string through friction. Rayleigh proved that the vibration could not be sustained under a normal friction law having a positive frictional coefficient. It is true even for a nonlinear friction with a positive coefficient in the first order term. In order to solve the problem, he modified the equation of motion for the string by introducing a negative first order coefficient and a positive third order coefficient. This approach is consistent at least in the sense of energetics, though a negative frictional coefficient is a bit unusual.

It turned out that the Rayleigh's equation of motion was equivalent to van der Pol's equation (Drazin, 1992), which had been analyzed deeply by decent researchers. We construct and summarize the behavior of Rayleigh type equation of motion for a setting suitable to seismic phenomena in the next section. In section 3, numerical studies for a coupled Rayleigh oscillators will be given. In section 4, a system of multiply connected Rayleigh oscillators will be studied and the system will be applied to seismic phenomena.

2. Single nonlinear oscillator

We consider a block placed on a conveying belt and connected to a fixed wall horizontally through a spring. The equation of motion is

$$\begin{aligned} m\ddot{x} &= -kx + F(v) \\ F(v) &= \mu_1 v - \mu_3 v^3 \\ v &= \dot{x} - V \end{aligned} \tag{1}$$

where $\mu_1 > 0$ and $\mu_3 > 0$ are the frictional coefficients introduced by Rayleigh, k is a spring constant and m the mass of the block. x is the position of the block measured from a fixed coordinate frame. V is driving velocity of the belt measured from the fixed frame. In general, F will be developed into a power

series of v. The constant term and terms of even power must be zero because the frictional force must be an odd function of the relative velocity v. We only retained first two non-zero terms. Behavior of a system with $\mu_1=0$ is qualitatively the same as a system with normal friction. Nonlinearity of the system (1) is determined by this quantity μ_1.

Introducing following transformation of variables to the equation (1),

$$\tau=\frac{\mu_1}{m}t,\ y=\frac{k}{\mu_1}\sqrt{\frac{\mu_3}{\mu_1}}x,\ u=\sqrt{\frac{\mu_3}{\mu_1}}v \tag{2}$$

we obtain a system of nonlinear ordinary differential equations

$$\begin{aligned}\frac{du}{d\tau}&=-y+u-u^3\\ \frac{dy}{d\tau}&=\varepsilon(u+a)\end{aligned} \tag{3}$$

where

$$\varepsilon=\frac{mK}{{\mu_1}^2},\ a=\sqrt{\frac{\mu_3}{\mu_1}}V \tag{4}$$

ε is a nonlinear parameter and a is a dimensionless driving velocity. When ε is small, the system is strongly nonlinear because larger μ_1 means stronger nonlinearity as stated above. The equation (3) is Rayleigh's equation of motion. Here after we call the motion of a block expressed by equation (3) a Rayleigh oscillator.

This system (3) has a fixed point at $(y^*,\ u^*)=(a^3-a,\ -a)$. Linearization of equation (3) at the fixed point gives a following system of equations;

$$\begin{aligned}\dot{x}&=\varepsilon v\\ \dot{v}&=-x+(1-3a^2)v\end{aligned} \tag{5}$$

where $y=y^*+x$, $u=u^*+v$. Eigenvalues of the coefficient matrix of equation (5) are given as

$$\lambda=\frac{1}{2}\left\{3a^2-1\pm\sqrt{(3a^2-1)^2-4\varepsilon}\right\} \tag{6}$$

From this we know that at $a=1/\sqrt{3}$, i.e., $Re(\lambda)=0$, the system undergoes Hopf bifurcation (see Drazin, 1992). This bifurcation point plays the most important part even for systems of multiply connected Rayleigh oscillators discussed in the later sections.

For slower driving velocity a than $1/\sqrt{3}$, the system has a limit cycle and for

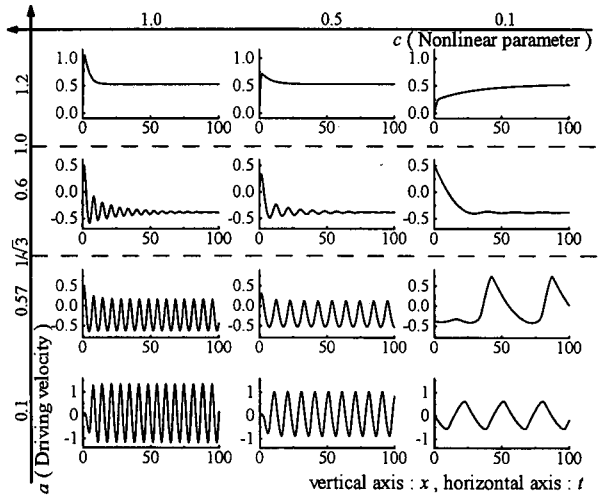

Fig. 1. Displacements of the block for different nonlinear parameter values and driving velocities. The system undergoes Hopf bifurcation at the driving velocity a of $1/\sqrt{3}$. For slower velocity than this, the system approaches a limit cycle motion (traces in the lower two rows). The "period" of the limit cycle increases as the nonlinear parameter decreases (increase of nonlinearity).

cases of $\frac{1}{\sqrt{3}}<a<\sqrt{\frac{2\sqrt{\varepsilon}+1}{3}}$, the system's motion is damped oscillation. For faster a than the range above, the system reaches a state of steady sliding without oscillation. These behaviors are illustrated in figure 1 which is constructed by numerical calculations of equation (3).

3. A coupled Rayleigh oscillators

(a) Equation of motion and elementary analyses

We couple two Rayleigh oscillators defined in section 2 by a linear spring and a slider. The reason that we employ linear coupling is only for simplicity. Equations of motion for the coupled oscillators may be

$$\begin{aligned}
\dot{u}_1&=-y_1+u_1-u_1^3-\nu(u_1-u_2)+\varkappa(y_2-y_1)\\
\dot{y}_1&=\varepsilon_1(u_1+a)\\
\dot{u}_2&=-y_2+u_2-u_2^3-\nu(u_2-u_1)+\varkappa(y_1-y_2)\\
\dot{y}_2&=\varepsilon_2(u_2+a)
\end{aligned}\tag{7}$$

where quantities with suffix 1 belong to the block 1 and so on. The viscous coupling coefficient is ν and the elastic coupling coefficient is $\varkappa$. The dimension-

less driving velocities for block 1 and 2 can be different but are taken to be the same a only for simplicity.

The system (7) has a fixed point at

$$\begin{aligned} u_1 &= -a,\ y_1 = a(a^2-1), \\ u_2 &= -a,\ y_2 = a(a^2-1) \end{aligned} \tag{8}$$

Linearization of equation (7) at the fixed point (8) gives a following Jacobian for the system

$$A = \begin{bmatrix} 1-3a^2-\nu & -1-\varkappa & \nu & \varkappa \\ \varepsilon_1 & 0 & 0 & 0 \\ \nu & \varkappa & 1-3a^2-\nu & -1-\varkappa \\ 0 & 0 & \varepsilon_2 & 0 \end{bmatrix} \tag{9}$$

Matrix A has four eigenvalues which can be obtained analytically but extremely messy. One of the eigenvalues is given in figure 2. We have to obtain transition or bifurcation points for driving velocity a as a function of given values of the nonlinear parameters and coupling constants numerically.

Here after, we give numerical results for cases with fixed parameters; two nonlinear parameters are fixed to be 0.4 and 0.3 and coupling constants ν and $\varkappa$ to be 0.1. With these values, a pair of the eigenvalues is real for $a \geqq 0.82486$, and the other for $a \geqq 0.86379$. Bifurcation points in the sense defined in two dimensional cases are $a=0.52480244$ and $a=0.56858196$. These are the points where each eigenvalue is pure imaginary. In the range of eigenvalues being real, the motion of the blocks approaches to a steady state without oscillation.

Figure 3 shows examples of traces of displacements and corresponding Lorenz maps (Strogatz, 1994) for one of the blocks. We can see that, for sufficiently low driving velocities, the Lorenz map is expressed by a closed curve, i.e., the motion is quasi-periodic. For around $a=0.53$, the mapping curves are quite complex. An example of the most striking and beautiful complex curves which actually consist of isolated points and have fractal structure is given in figure 4. Such a complex curve is generated by folding consecutively a simple closed curve as a increases. Such a folding is first observed near a point of $a=0.46$. Between $a=0.3$ and 0.42, Lorenz points converge to a single point. This suggests an existence of a simple four dimensional limit cycle in this range of the driving velocity. Between $a=0.42$ and 0.46, Lorenz points make a closed curve. This suggests a quasi-periodic orbit.

In figure 5, a bifurcation diagram is shown for the displacements of the

```
1/2 (1 - 3 a^2 - v) - 1/2 √(-1 + 6 a^2 - 9 a^4 + 2 v - 6 a^2 v +
    (-1 + 3 a^2 + v)^2 - ε1 - κ ε1 - ε2 - κ ε2 + 1/3 (1 - 6 a^2 + 9 a^4 - 2 v + 6 a^2 v + ε1 + κ ε1 + ε2 + κ ε2) +
    (2^(1/3) (12 (1 + 2 κ) ε1 ε2 + (1 - 6 a^2 + 9 a^4 - 2 v + 6 a^2 v + ε1 + κ ε1 + ε2 + κ ε2)^2 -
       6 (-1 + 3 a^2 + v) (-ε1 + 3 a^2 ε1 - κ ε1 + 3 a^2 κ ε1 + v ε1 - ε2 + 3 a^2 ε2 - κ ε2 + 3 a^2 κ ε2 + v ε2)))/
     (3 (108 (1 + 2 κ) (-1 + 3 a^2 + v)^2 ε1 ε2 -
        72 (1 + 2 κ) ε1 ε2 (1 - 6 a^2 + 9 a^4 - 2 v + 6 a^2 v + ε1 + κ ε1 + ε2 + κ ε2) +
        2 (1 - 6 a^2 + 9 a^4 - 2 v + 6 a^2 v + ε1 + κ ε1 + ε2 + κ ε2)^3 -
        18 (-1 + 3 a^2 + v) (1 - 6 a^2 + 9 a^4 - 2 v + 6 a^2 v + ε1 + κ ε1 + ε2 + κ ε2)
         (-ε1 + 3 a^2 ε1 - κ ε1 + 3 a^2 κ ε1 + v ε1 - ε2 + 3 a^2 ε2 - κ ε2 + 3 a^2 κ ε2 + v ε2) +
        27 (-ε1 + 3 a^2 ε1 - κ ε1 + 3 a^2 κ ε1 + v ε1 - ε2 + 3 a^2 ε2 - κ ε2 + 3 a^2 κ ε2 + v ε2)^2 +
        √(-4 (12 (1 + 2 κ) ε1 ε2 + (1 - 6 a^2 + 9 a^4 - 2 v + 6 a^2 v + ε1 + κ ε1 + ε2 + κ ε2)^2 - 6 (-1 + 3 a^2 + v)
             (-ε1 + 3 a^2 ε1 - κ ε1 + 3 a^2 κ ε1 + v ε1 - ε2 + 3 a^2 ε2 - κ ε2 + 3 a^2 κ ε2 + v ε2)))^3 +
          (108 (1 + 2 κ) (-1 + 3 a^2 + v)^2 ε1 ε2 -
           72 (1 + 2 κ) ε1 ε2 (1 - 6 a^2 + 9 a^4 - 2 v + 6 a^2 v + ε1 + κ ε1 + ε2 + κ ε2) +
           2 (1 - 6 a^2 + 9 a^4 - 2 v + 6 a^2 v + ε1 + κ ε1 + ε2 + κ ε2)^3 -
           18 (-1 + 3 a^2 + v) (1 - 6 a^2 + 9 a^4 - 2 v + 6 a^2 v + ε1 + κ ε1 + ε2 + κ ε2)
            (-ε1 + 3 a^2 ε1 - κ ε1 + 3 a^2 κ ε1 + v ε1 - ε2 + 3 a^2 ε2 - κ ε2 + 3 a^2 κ ε2 + v ε2) +
           27 (-ε1 + 3 a^2 ε1 - κ ε1 + 3 a^2 κ ε1 + v ε1 - ε2 + 3 a^2 ε2 - κ ε2 + 3 a^2 κ ε2 + v ε2)^2)^2))^
       (1/3)) +
  1/(3 2^(1/3))
   ((108 (1 + 2 κ) (-1 + 3 a^2 + v)^2 ε1 ε2 - 72 (1 + 2 κ) ε1 ε2 (1 - 6 a^2 + 9 a^4 - 2 v + 6 a^2 v + ε1 + κ ε1 + ε2 + κ ε2) +
      2 (1 - 6 a^2 + 9 a^4 - 2 v + 6 a^2 v + ε1 + κ ε1 + ε2 + κ ε2)^3 -
      18 (-1 + 3 a^2 + v) (1 - 6 a^2 + 9 a^4 - 2 v + 6 a^2 v + ε1 + κ ε1 + ε2 + κ ε2)
       (-ε1 + 3 a^2 ε1 - κ ε1 + 3 a^2 κ ε1 + v ε1 - ε2 + 3 a^2 ε2 - κ ε2 + 3 a^2 κ ε2 + v ε2) +
      27 (-ε1 + 3 a^2 ε1 - κ ε1 + 3 a^2 κ ε1 + v ε1 - ε2 + 3 a^2 ε2 - κ ε2 + 3 a^2 κ ε2 + v ε2)^2 +
      √(-4 (12 (1 + 2 κ) ε1 ε2 + (1 - 6 a^2 + 9 a^4 - 2 v + 6 a^2 v + ε1 + κ ε1 + ε2 + κ ε2)^2 -
           6 (-1 + 3 a^2 + v) (-ε1 + 3 a^2 ε1 - κ ε1 + 3 a^2 κ ε1 + v ε1 - ε2 + 3 a^2 ε2 - κ ε2 + 3 a^2 κ ε2 + v ε2)))^3 +
        (108 (1 + 2 κ) (-1 + 3 a^2 + v)^2 ε1 ε2 -
         72 (1 + 2 κ) ε1 ε2 (1 - 6 a^2 + 9 a^4 - 2 v + 6 a^2 v + ε1 + κ ε1 + ε2 + κ ε2) +
         2 (1 - 6 a^2 + 9 a^4 - 2 v + 6 a^2 v + ε1 + κ ε1 + ε2 + κ ε2)^3 -
         18 (-1 + 3 a^2 + v) (1 - 6 a^2 + 9 a^4 - 2 v + 6 a^2 v + ε1 + κ ε1 + ε2 + κ ε2)
          (-ε1 + 3 a^2 ε1 - κ ε1 + 3 a^2 κ ε1 + v ε1 - ε2 + 3 a^2 ε2 - κ ε2 + 3 a^2 κ ε2 + v ε2) +
         27 (-ε1 + 3 a^2 ε1 - κ ε1 + 3 a^2 κ ε1 + v ε1 - ε2 + 3 a^2 ε2 - κ ε2 + 3 a^2 κ ε2 + v ε2)^2)^2)^
     (1/3)) -
1/2 √(-1 + 6 a^2 - 9 a^4 + 2 v - 6 a^2 v +
    2 (-1 + 3 a^2 + v)^2 - ε1 - κ ε1 - ε2 - κ ε2 + 1/3 (-1 + 6 a^2 - 9 a^4 + 2 v - 6 a^2 v - ε1 - κ ε1 - ε2 - κ ε2) -
    (2^(1/3) (12 (1 + 2 κ) ε1 ε2 + (1 - 6 a^2 + 9 a^4 - 2 v + 6 a^2 v + ε1 + κ ε1 + ε2 + κ ε2)^2 -
       6 (-1 + 3 a^2 + v) (-ε1 + 3 a^2 ε1 - κ ε1 + 3 a^2 κ ε1 + v ε1 - ε2 + 3 a^2 ε2 - κ ε2 + 3 a^2 κ ε2 + v ε2)))/
     (3 (108 (1 + 2 κ) (-1 + 3 a^2 + v)^2 ε1 ε2 -
        72 (1 + 2 κ) ε1 ε2 (1 - 6 a^2 + 9 a^4 - 2 v + 6 a^2 v + ε1 + κ ε1 + ε2 + κ ε2) +
        2 (1 - 6 a^2 + 9 a^4 - 2 v + 6 a^2 v + ε1 + κ ε1 + ε2 + κ ε2)^3 -
        18 (-1 + 3 a^2 + v) (1 - 6 a^2 + 9 a^4 - 2 v + 6 a^2 v + ε1 + κ ε1 + ε2 + κ ε2)
         (-ε1 + 3 a^2 ε1 - κ ε1 + 3 a^2 κ ε1 + v ε1 - ε2 + 3 a^2 ε2 - κ ε2 + 3 a^2 κ ε2 + v ε2) + 27 (-ε1 + 3 a^2 ε1 - κ ε1 +
          3 a^2 κ ε1 + v ε1 - ε2 + 3 a^2 ε2 - κ ε2 + 3 a^2 κ ε2 + v ε2)^2 + √(-4 (12 (1 + 2 κ) ε1 ε2 +
            (1 - 6 a^2 + 9 a^4 - 2 v + 6 a^2 v + ε1 + κ ε1 + ε2 + κ ε2)^2 - 6 (-1 + 3 a^2 + v) (-ε1 + 3 a^2 ε1 - κ ε1 +
              3 a^2 κ ε1 + v ε1 - ε2 + 3 a^2 ε2 - κ ε2 + 3 a^2 κ ε2 + v ε2)))^3 + (108 (1 + 2 κ) (-1 + 3 a^2 + v)^2
           ε1 ε2 - 72 (1 + 2 κ) ε1 ε2 (1 - 6 a^2 + 9 a^4 - 2 v + 6 a^2 v + ε1 + κ ε1 + ε2 + κ ε2) +
          2 (1 - 6 a^2 + 9 a^4 - 2 v + 6 a^2 v + ε1 + κ ε1 + ε2 + κ ε2)^3 -
          18 (-1 + 3 a^2 + v) (1 - 6 a^2 + 9 a^4 - 2 v + 6 a^2 v + ε1 + κ ε1 + ε2 + κ ε2)
           (-ε1 + 3 a^2 ε1 - κ ε1 + 3 a^2 κ ε1 + v ε1 - ε2 + 3 a^2 ε2 - κ ε2 + 3 a^2 κ ε2 + v ε2) +
          27 (-ε1 + 3 a^2 ε1 - κ ε1 + 3 a^2 κ ε1 + v ε1 - ε2 + 3 a^2 ε2 - κ ε2 + 3 a^2 κ ε2 + v ε2)^2)^2)^
     (1/3)) -
  1/(3 2^(1/3))
   ((108 (1 + 2 κ) (-1 + 3 a^2 + v)^2 ε1 ε2 - 72 (1 + 2 κ) ε1 ε2 (1 - 6 a^2 + 9 a^4 - 2 v + 6 a^2 v + ε1 + κ ε1 + ε2 + κ ε2) +
      2 (1 - 6 a^2 + 9 a^4 - 2 v + 6 a^2 v + ε1 + κ ε1 + ε2 + κ ε2)^3 -
      18 (-1 + 3 a^2 + v) (1 - 6 a^2 + 9 a^4 - 2 v + 6 a^2 v + ε1 + κ ε1 + ε2 + κ ε2)
```

Fig. 2-1

$$
\begin{aligned}
&(-\epsilon_1 + 3a^2\epsilon_1 - \kappa\epsilon_1 + 3a^2\kappa\epsilon_1 + \nu\epsilon_1 - \epsilon_2 + 3a^2\epsilon_2 - \kappa\epsilon_2 + 3a^2\kappa\epsilon_2 + \nu\epsilon_2) + \\
&27\,(-\epsilon_1 + 3a^2\epsilon_1 - \kappa\epsilon_1 + 3a^2\kappa\epsilon_1 + \nu\epsilon_1 - \epsilon_2 + 3a^2\epsilon_2 - \kappa\epsilon_2 + 3a^2\kappa\epsilon_2 + \nu\epsilon_2)^2 + \\
&\sqrt{(-4\,(12\,(1+2\kappa)\,\epsilon_1\epsilon_2 + (1-6a^2+9a^4-2\nu+6a^2\nu+\epsilon_1+\kappa\epsilon_1+\epsilon_2+\kappa\epsilon_2)^2 - 6\,(-1+3a^2+\nu)} \\
&\qquad (-\epsilon_1 + 3a^2\epsilon_1 - \kappa\epsilon_1 + 3a^2\kappa\epsilon_1 + \nu\epsilon_1 - \epsilon_2 + 3a^2\epsilon_2 - \kappa\epsilon_2 + 3a^2\kappa\epsilon_2 + \nu\epsilon_2))^3 + (108\,(1+2\kappa) \\
&\qquad (-1+3a^2+\nu)^2\,\epsilon_1\epsilon_2 - 72\,(1+2\kappa)\,\epsilon_1\epsilon_2\,(1-6a^2+9a^4-2\nu+6a^2\nu+\epsilon_1+\kappa\epsilon_1+\epsilon_2+\kappa\epsilon_2) + \\
&\qquad 2\,(1-6a^2+9a^4-2\nu+6a^2\nu+\epsilon_1+\kappa\epsilon_1+\epsilon_2+\kappa\epsilon_2)^3 - \\
&\qquad 18\,(-1+3a^2+\nu)\,(1-6a^2+9a^4-2\nu+6a^2\nu+\epsilon_1+\kappa\epsilon_1+\epsilon_2+\kappa\epsilon_2) \\
&\qquad (-\epsilon_1 + 3a^2\epsilon_1 - \kappa\epsilon_1 + 3a^2\kappa\epsilon_1 + \nu\epsilon_1 - \epsilon_2 + 3a^2\epsilon_2 - \kappa\epsilon_2 + 3a^2\kappa\epsilon_2 + \nu\epsilon_2) + \\
&\qquad 27\,(-\epsilon_1 + 3a^2\epsilon_1 - \kappa\epsilon_1 + 3a^2\kappa\epsilon_1 + \nu\epsilon_1 - \epsilon_2 + 3a^2\epsilon_2 - \kappa\epsilon_2 + 3a^2\kappa\epsilon_2 + \nu\epsilon_2)^2)^2))^{(1/3)} - \\
&(-8\,(-1+3a^2+\nu)^3 + 8\,(-1+3a^2+\nu)\,(1-6a^2+9a^4-2\nu+6a^2\nu+\epsilon_1+\kappa\epsilon_1+\epsilon_2+\kappa\epsilon_2) - \\
&\quad 8\,(-\epsilon_1 + 3a^2\epsilon_1 - \kappa\epsilon_1 + 3a^2\kappa\epsilon_1 + \nu\epsilon_1 - \epsilon_2 + 3a^2\epsilon_2 - \kappa\epsilon_2 + 3a^2\kappa\epsilon_2 + \nu\epsilon_2))\Big/ \\
&(4\sqrt{(-1+6a^2-9a^4+2\nu-6a^2\nu+(-1+3a^2+\nu)^2 - \epsilon_1 - \kappa\epsilon_1 - \epsilon_2 - } \\
&\quad \kappa\epsilon_2 + \tfrac{1}{3}\,(1-6a^2+9a^4-2\nu+6a^2\nu+\epsilon_1+\kappa\epsilon_1+\epsilon_2+\kappa\epsilon_2) + (2^{1/3}\,(12\,(1+2\kappa)\,\epsilon_1\epsilon_2 + \\
&\qquad (1-6a^2+9a^4-2\nu+6a^2\nu+\epsilon_1+\kappa\epsilon_1+\epsilon_2+\kappa\epsilon_2)^2 - 6\,(-1+3a^2+\nu)\,(-\epsilon_1 + 3a^2\epsilon_1 - \kappa\epsilon_1 + \\
&\qquad 3a^2\kappa\epsilon_1 + \nu\epsilon_1 - \epsilon_2 + 3a^2\epsilon_2 - \kappa\epsilon_2 + 3a^2\kappa\epsilon_2 + \nu\epsilon_2)))\Big/(3\,(108\,(1+2\kappa) \\
&\qquad (-1+3a^2+\nu)^2\,\epsilon_1\epsilon_2 - 72\,(1+2\kappa)\,\epsilon_1\epsilon_2\,(1-6a^2+9a^4-2\nu+6a^2\nu+\epsilon_1+\kappa\epsilon_1+\epsilon_2+\kappa\epsilon_2) + \\
&\qquad 2\,(1-6a^2+9a^4-2\nu+6a^2\nu+\epsilon_1+\kappa\epsilon_1+\epsilon_2+\kappa\epsilon_2)^3 - 18\,(-1+3a^2+\nu) \\
&\qquad (1-6a^2+9a^4-2\nu+6a^2\nu+\epsilon_1+\kappa\epsilon_1+\epsilon_2+\kappa\epsilon_2)\,(-\epsilon_1 + 3a^2\epsilon_1 - \kappa\epsilon_1 + 3a^2\kappa \\
&\qquad \epsilon_1 + \nu\epsilon_1 - \epsilon_2 + 3a^2\epsilon_2 - \kappa\epsilon_2 + 3a^2\kappa\epsilon_2 + \nu\epsilon_2) + 27\,(-\epsilon_1 + 3a^2\epsilon_1 - \kappa\epsilon_1 + 3 \\
&\qquad a^2\kappa\epsilon_1 + \nu\epsilon_1 - \epsilon_2 + 3a^2\epsilon_2 - \kappa\epsilon_2 + 3a^2\kappa\epsilon_2 + \nu\epsilon_2)^2 + \sqrt{(-4\,(12\,(1+2 \\
&\qquad\qquad \kappa)\,\epsilon_1\epsilon_2 + (1-6a^2+9a^4-2\nu+6a^2\nu+\epsilon_1+\kappa\epsilon_1+\epsilon_2+\kappa\epsilon_2)^2 - 6\,(-1+3 \\
&\qquad\qquad a^2+\nu)\,(-\epsilon_1 + 3a^2\epsilon_1 - \kappa\epsilon_1 + 3a^2\kappa\epsilon_1 + \nu\epsilon_1 - \epsilon_2 + 3a^2\epsilon_2 - \kappa\epsilon_2 + 3a^2\kappa\epsilon_2 + \nu \\
&\qquad\qquad \epsilon_2))^3 + (108\,(1+2\kappa)\,(-1+3a^2+\nu)^2\,\epsilon_1\epsilon_2 - 72\,(1+2\kappa)\,\epsilon_1\epsilon_2\,(1-6a^2+9 \\
&\qquad\qquad a^4-2\nu+6a^2\nu+\epsilon_1+\kappa\epsilon_1+\epsilon_2+\kappa\epsilon_2) + 2\,(1-6a^2+9a^4-2\nu+6a^2\nu+\epsilon_1+\kappa \\
&\qquad\qquad \epsilon_1+\epsilon_2+\kappa\epsilon_2)^3 - 18\,(-1+3a^2+\nu)\,(1-6a^2+9a^4-2\nu+6a^2\nu+\epsilon_1+\kappa \\
&\qquad\qquad \epsilon_1+\epsilon_2+\kappa\epsilon_2)\,(-\epsilon_1 + 3a^2\epsilon_1 - \kappa\epsilon_1 + 3a^2\kappa\epsilon_1 + \nu\epsilon_1 - \epsilon_2 + 3a^2\epsilon_2 - \kappa\epsilon_2 + 3a^2\kappa \\
&\qquad\qquad \epsilon_2 + \nu\epsilon_2) + 27\,(-\epsilon_1 + 3a^2\epsilon_1 - \kappa\epsilon_1 + 3a^2\kappa\epsilon_1 + \nu\epsilon_1 - \epsilon_2 + 3a^2\epsilon_2 - \kappa \\
&\qquad\qquad \epsilon_2 + 3a^2\kappa\epsilon_2 + \nu\epsilon_2)^2))^2))^{(1/3)} + \frac{1}{3\,2^{1/3}}\,((108\,(1+2\kappa)\,(-1+3a^2+\nu)^2 \\
&\quad \epsilon_1\epsilon_2 - 72\,(1+2\kappa)\,\epsilon_1\epsilon_2\,(1-6a^2+9a^4-2\nu+6a^2\nu+\epsilon_1+\kappa\epsilon_1+\epsilon_2+\kappa\epsilon_2) + \\
&\quad 2\,(1-6a^2+9a^4-2\nu+6a^2\nu+\epsilon_1+\kappa\epsilon_1+\epsilon_2+\kappa\epsilon_2)^3 - 18\,(-1+3a^2+\nu) \\
&\quad (1-6a^2+9a^4-2\nu+6a^2\nu+\epsilon_1+\kappa\epsilon_1+\epsilon_2+\kappa\epsilon_2)\,(-\epsilon_1 + 3a^2\epsilon_1 - \kappa\epsilon_1 + 3a^2\kappa\epsilon_1 + \nu\epsilon_1 - \epsilon_2 + \\
&\quad 3a^2\epsilon_2 - \kappa\epsilon_2 + 3a^2\kappa\epsilon_2 + \nu\epsilon_2) + 27\,(-\epsilon_1 + 3a^2\epsilon_1 - \kappa\epsilon_1 + 3a^2\kappa\epsilon_1 + \nu\epsilon_1 - \epsilon_2 + \\
&\quad 3a^2\epsilon_2 - \kappa\epsilon_2 + 3a^2\kappa\epsilon_2 + \nu\epsilon_2)^2 + \sqrt{(-4\,(12\,(1+2\kappa)\,\epsilon_1\epsilon_2 + (1-6a^2+9a^4-2 \\
&\qquad \nu+6a^2\nu+\epsilon_1+\kappa\epsilon_1+\epsilon_2+\kappa\epsilon_2)^2 - 6\,(-1+3a^2+\nu)\,(-\epsilon_1 + 3a^2\epsilon_1 - \kappa\epsilon_1 + 3 \\
&\qquad a^2\kappa\epsilon_1 + \nu\epsilon_1 - \epsilon_2 + 3a^2\epsilon_2 - \kappa\epsilon_2 + 3a^2\kappa\epsilon_2 + \nu\epsilon_2))^3 + (108\,(1+2 \\
&\qquad \kappa)\,(-1+3a^2+\nu)^2\,\epsilon_1\epsilon_2 - 72\,(1+2\kappa)\,\epsilon_1\epsilon_2\,(1-6a^2+9a^4-2\nu+6a^2\nu+\epsilon_1+\kappa \\
&\qquad \epsilon_1+\epsilon_2+\kappa\epsilon_2) + 2\,(1-6a^2+9a^4-2\nu+6a^2\nu+\epsilon_1+\kappa\epsilon_1+\epsilon_2+\kappa\epsilon_2)^3 - 18\,(-1+ \\
&\qquad 3a^2+\nu)\,(1-6a^2+9a^4-2\nu+6a^2\nu+\epsilon_1+\kappa\epsilon_1+\epsilon_2+\kappa\epsilon_2)\,(-\epsilon_1 + 3a^2\epsilon_1 - \kappa\epsilon_1 + 3a^2 \\
&\qquad \kappa\epsilon_1 + \nu\epsilon_1 - \epsilon_2 + 3a^2\epsilon_2 - \kappa\epsilon_2 + 3a^2\kappa\epsilon_2 + \nu\epsilon_2) + 27\,(-\epsilon_1 + 3a^2\epsilon_1 - \kappa \\
&\qquad \epsilon_1 + 3a^2\kappa\epsilon_1 + \nu\epsilon_1 - \epsilon_2 + 3a^2\epsilon_2 - \kappa\epsilon_2 + 3a^2\kappa\epsilon_2 + \nu\epsilon_2)^2)^2))^{(1/3)})))
\end{aligned}
$$

Fig. 2-2

Fig. 2. Analytic expression of an eigenvalue of the linearized coefficient matrix at the fixed point of the coupled Rayleigh oscillators.

block which has a nonlinear parameter $\varepsilon_1 = 0.4$. The structure of the diagram is extremely complex but some regularities can be seen. There are clear periodic windows which contain a typical bifurcation structure of the period doubling sequence. An example of this bifurcation is shown in figure 6 which is an enlarged version of figure 5. This suggests that there is a region of the driving velocity where chaotic orbits appear. Bifurcations or period doubling patterns develop into both directions, a increasing and a decreasing. We don't know what mechanisms determine the directions. This bidirectional develop-

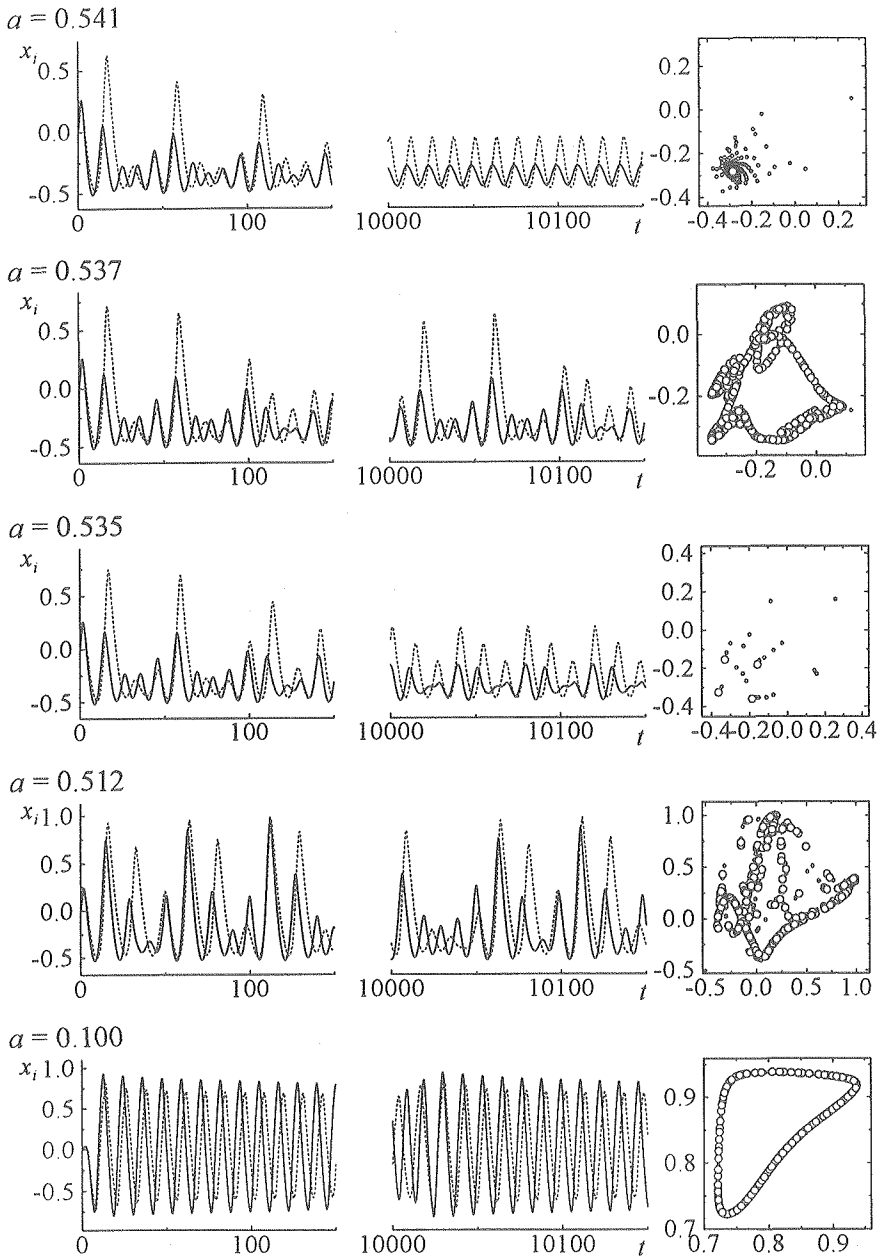

Fig. 3. Traces of motions of two blocks and their Lorenz maps obtained from peak displacement amplitudes of one of the blocks. The Lorenz maps are depicted in squares in the right most column. Each map was obtained from the traces placed in the same row, which is calculated at the assigned driving velocity a.

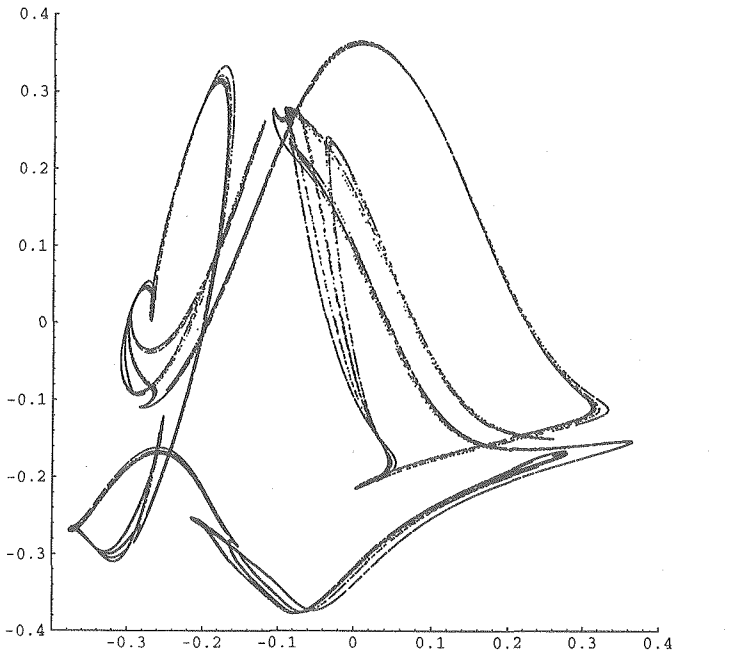

Fig. 4. An example of Lorenz map (iterated map) showing fractal structure calculated for a coupled Rayleigh oscillators forced at the driving velocity of 0.53.

ment of the doubling sequence-like pattern suggests that a range of the driving velocity in between the periodic windows may not necessarily correspond to a chaotic (infinitely many periodic) state.

For cases with large ε's (weak nonlinearity), only closed curves appear in the Lorenz maps. Yokomori (1997) gave some of the case studies by numerical integration. It is difficult to find exactly where the folding begins to occur through numerical integration. What we have made so far are standard and elementary analyses in the nonlinear science. Next we study other aspect of the motion of the system.

(b) Statistical nature

Gutenberg-Richiter relation for seismic activity is a linear relation between logarithm of frequency of earthquake occurrence and the magnitude. This is one of the so-called inverse power laws hold in many complex systems. We can expect that our system of Rayleigh oscillators has an inverse power character because of its chaotic motion in some range of driving velocities.

Earthquake magnitude is proportional to logarithm of the displacement of a dislocation (an earthquake fault) multiplied by other factors (see Utsu, 1977).

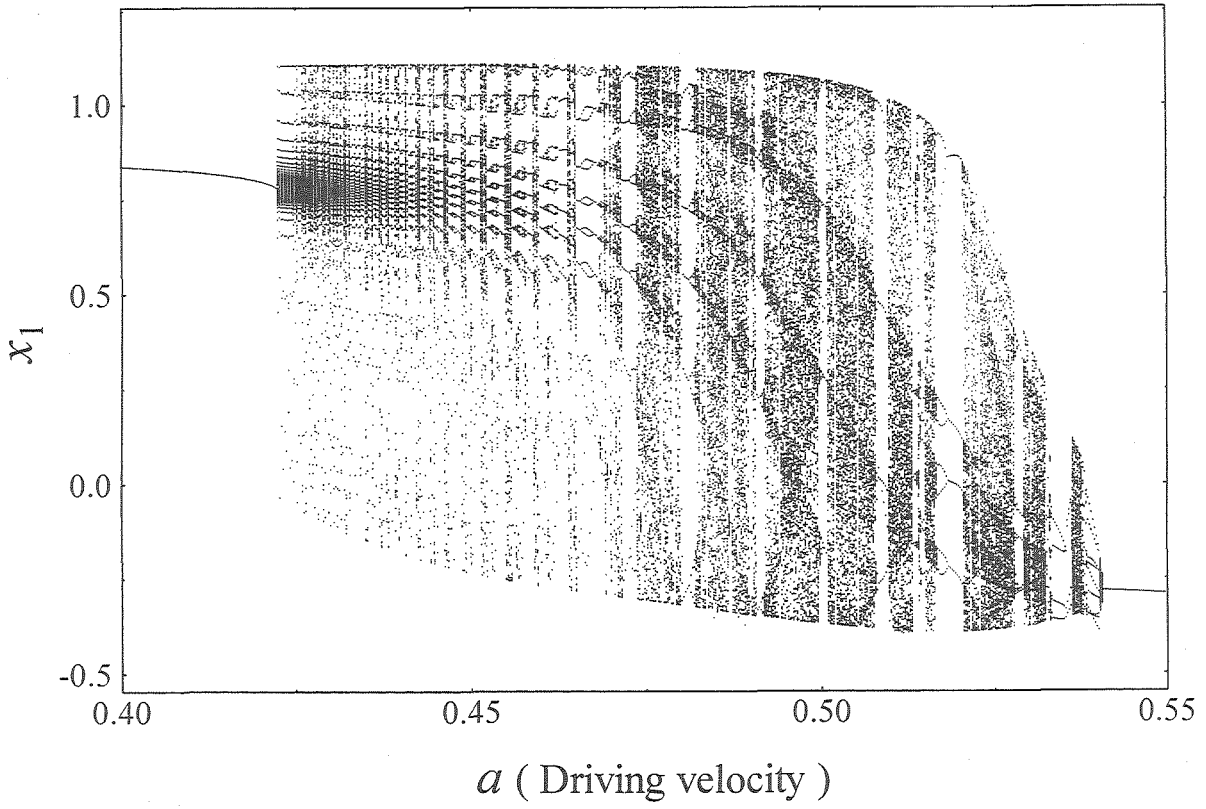

Fig. 5. Bifurcation diagram of a coupled Rayleigh oscillators. Periodic windows and some regularities are clearly seen. Bifurcations occur in both directions of a increases and decreases.

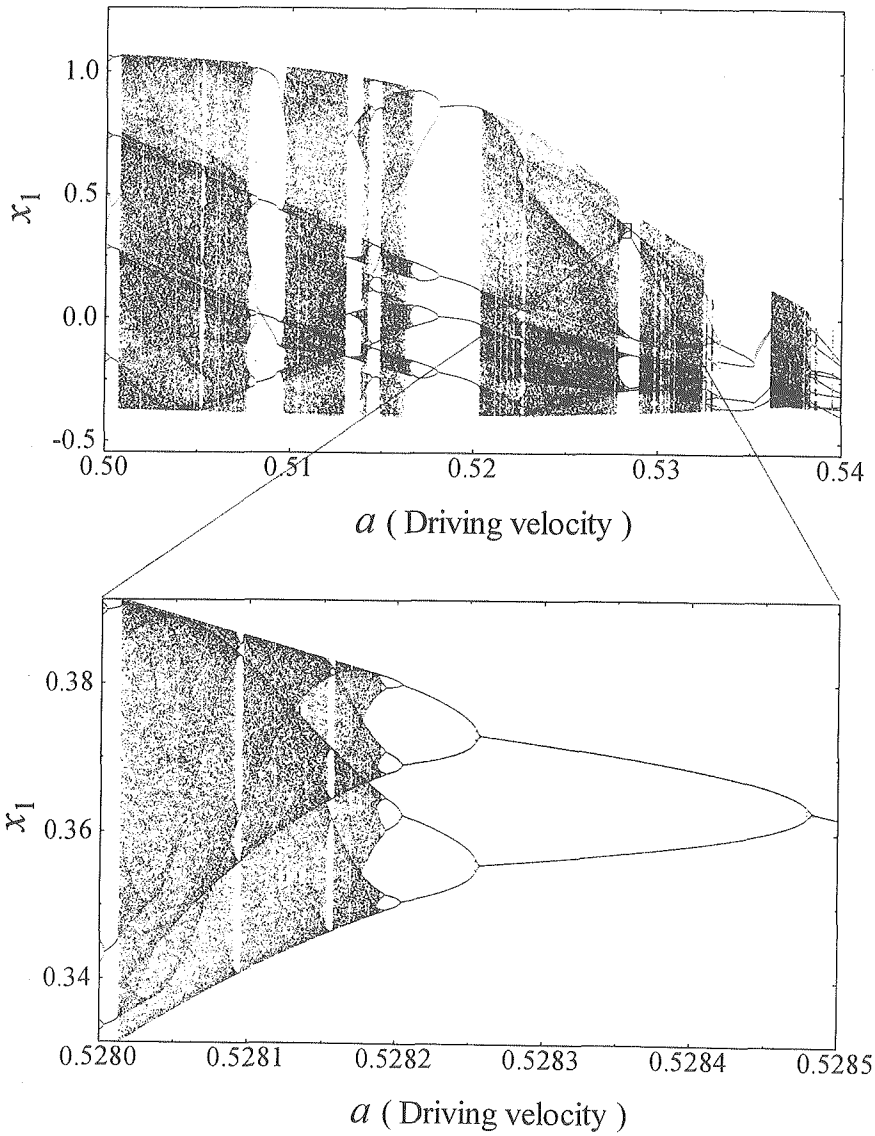

Fig. 6. Enlarged diagrams of Fig. 5. The lower diagram shows the famous bifurcation structure of period doubling sequence and is a greatly enlarged portion of the upper one. From this diagram, we can expect the behavior of the coupled Rayleigh oscillators to be chaotic at least in some range of the driving velocity.

We define a magnitude for our system as logarithm of the displacement amplitude of a block. Then the magnitude-frequency relation is calculated as follow: Calculate displacements of one of the blocks as a function of time. Find local maxima (we call them peak and also events) and record peak amplitudes measured from a prefixed base line. Count the number of peaks having an assigned range of amplitude. It is not needed at this point a physical scaling factor for the relation, thanks to the logarithmic nature.

An example of the magnitude-frequency relation thus obtained is shown in figure 7. A linear relation holds only on average and in a limited range of magnitude because of the numerical resolution. The variance is large but will be reduced if we employ many Rayleigh oscillators as will be given in the next section. Our system actually has the statistical nature expressed by an inverse power law, though this law holds only within very restricted values of the driving velocity.

4. Multiply connected Rayleigh oscillators

(a) Statistical nature of the model system

In this section, we examine what happens when we increase the number of Rayleigh oscillators. We take the same linear coupling mechanism between adjacent blocks as the case of two blocks stated in the preceding section. Then the equation of motion of the i-th block is read as

$$\begin{aligned}\dot{u} &= -y_i + u_i - u_i^3 + \nu_{i-1}(u_{i-1} - u_i) - \nu_i(u_i - u_{i+1}) \\ &\quad + \chi_{i-1}(y_{i-1} - y_i) - \chi_i(y_i - y_{i+1}) \\ \dot{y}_i &= \varepsilon_i(u_i + a_i)\end{aligned} \tag{10}$$

where ν_i and χ_i are the viscous and elastic coupling coefficients between the i-th and (i+1)-th blocks, respectively. ε_i is the nonlinear parameter of the i-th Rayleigh oscillator. The dimensionless driving velocity a_i can be different from a block to block but are assumed to be equal in the following only for simplicity. We will give results for systems consisting of ten, twenty, and thirty blocks.

Because the behaviors of the systems are too complex to be analyzed through elementary techniques, we only examine the statistical nature with the same method stated in the second subsection of the precedent section. We also examined the effects of boundary conditions, open and cyclic. For details, see Yokomori (1997). All ν_i and χ_i are fixed to be 0.1 throughout for simplicity. The nonlinear parameters ε_i are determined so that εs distribute randomly

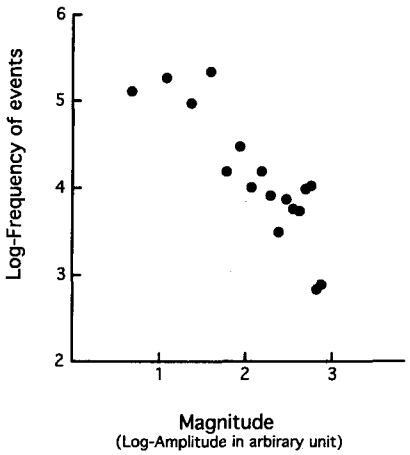

Fig. 7. Magnitude-frequency relation for the coupled Rayleigh oscillators. The magnitude is defined to be proportional to logarithm of the peak amplitude of displacement of a block. The unit is arbitrary. A linear relation (called Gutenberg-Richiter relation in seismology) holds approximately.

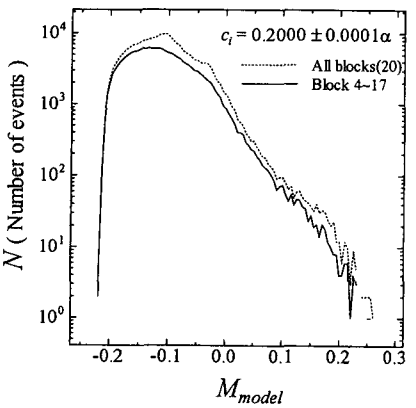

Fig. 8. Magnitude-frequency relation for a system consisting of twenty Rayleigh oscillators which are connected linearly with free boundary condition at both ends. This is much more smooth than that given in Fig. 7. A system consisting of the larger number of the oscillators gives a more smooth relation.

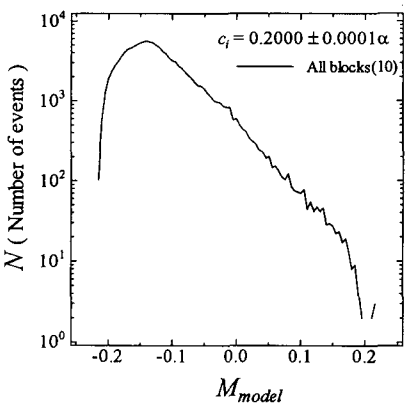

Fig. 9. Magnitude-frequency relation for a system consisting of ten Rayleigh oscillators connected linearly and cyclically. The effect of the cyclic boundary condition is not trivial. We obtain much more smooth relation with only half of the oscillators (compare to Fig. 8).

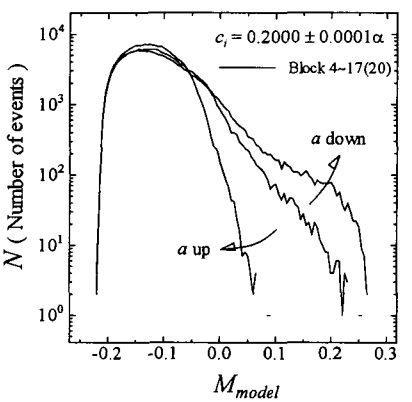

Fig. 10. Inclinations in the magnitude-frequency relation at and around the optimal value of the driving velocity a. The faster velocity gives steeper inclinations. The trend is affected neither by boundary conditions nor the number of oscillators.

around a given value. The variance is taken to be 0.0001 and the center value of the εs is 0.2. Even this very small variation of the nonlinear parameters results in a extremely complex behavior of the system.

We can certainly find a range of the driving velocity for which the system shows the inverse power law relation (here after M-F relation for short). The twenty blocks is sufficient to get a smooth M-F relation for an open boundary condition (see Figure 8). For the cyclic boundary condition, a system with ten blocks also shows the very smooth relation (figure 9). The inclination of the linear M-F relation varies as the driving velocity varies. An example of the variation is shown in figure 10 for a case of twenty blocks with open boundary conditions. For this case, the faster velocities a result in steeper inclinations. Without scaling the model system, we cannot compare the absolute value of the model system to the so-called b-value in seismology.

Next we examine the return period of events which is defined by

$$\tau := T(M) = 1/N(M) \tag{11}$$

where $N(M)$ is the total number of events larger than given magnitude M (Utsu, 1977). If a system behaves as a Poisson process, logarithm of the number of events having the return period τ, $N(\tau)$, is linearly proportional to the return period. It is known for natural seismic events that this linear relation approximately holds. For a branching process, $N(\tau)$ deviates from the linear trend at small τ. Figure 11 shows the $\log(N(\tau))$-τ relation together with M-F relation for case of 30 blocks with the cyclic boundary condition. The linearity is evident and the deviation is very small. For a system with the smaller number of blocks, the linearity is well established but deviations become larger. For the details of the effects of the number of blocks and the boundary conditions, see Yokomori (1997). We call this linear relation the return period-frequency relation or RP-F relation for short.

Now we can scale our system of Rayleigh oscillators; magnitude scaling and time scaling. To this end we make two comparisons between the M-F relation of a model system and that of real data and between the RP-F relations of those. We calculate the scaled magnitude M and time T from pre-scaled ones M' and T' by the following relations;

$$\begin{aligned} M &= BM' + c \\ B &:= \frac{b'}{b},\ c := M_{\min} - BM'_{\min} \\ T &:= \frac{\langle \tau \rangle}{\langle \tau' \rangle} T' \end{aligned} \tag{12}$$

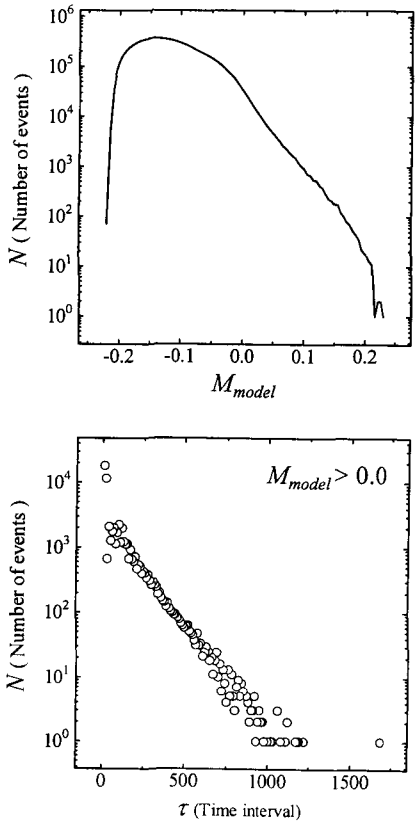

Fig. 11. Magnitude-frequency relation and return period-frequency (RP-F for short) relation calculated for the system of 30 oscillators under the cyclic boundary condition. The return period τ is denoted as time interval in the lower figure. The return period is analyzed for events having magnitude M_{model} greater than 0. The linearity in the RP-F relation is remarkably good. This model is used to analyze long term behaviors of the system of multiple Rayleigh oscillators and to compare with real seismic data.

where b is the inclination (b-value) and τ the return period. $\langle\ \rangle$ means the average and prime (') indicates pre-scaled (model) quantities. Because b and τ are the observed values and are specific to a region and period, the scaling (12) must be calculated for each region and period of interest. $(\ )_{\min}$ means the minimum value of the quantity inside the ( ). We also calculate "energy" release E by model events through the following equation;

$$E' := 10^c\, E'^B \tag{13}$$

where c and B are defined in (12) and E' is pre-scaled "energy" of a event having magnitude M'.

Observed period of seismic data are limited but the model data can be calculated as long as we want. Figure 12 shows a cumulative energy release of a model system. In order to retain the resolution of energy jump, the cumulation curve is switched to the bottom when time passed for given amount and, at the same time, the time origin is shifted. The given time length is 50000 in the calculation unit. This cumulation curve remind us of real seismic ones. The calculation was made for a model system consisting of 30 blocks with parameter values which resulted in a chaotic motion stated above.

We are interested in the question if the system has an ergodic nature. We only examine numerically recurrence nature. To this end, we prepare model data for sufficiently long time span as given figure 12.

(1) Select a portion of the curve and shift it along the original one.

(2) Calculate a correlation coefficient between selected data and shifted

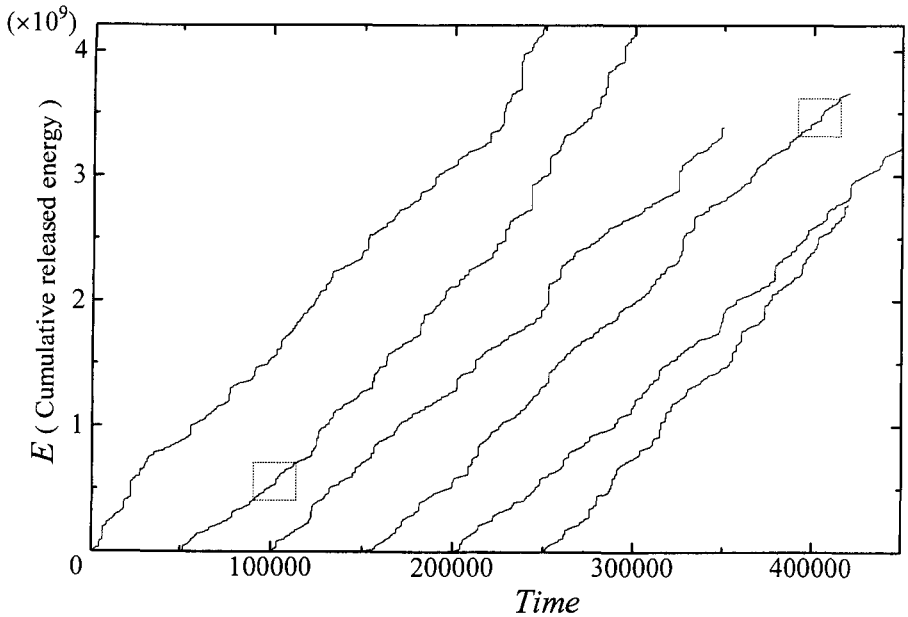

Fig. 12. Energy cumulation curve of the model system given in Fig. 11. In order to keep sufficient resolution for steps (energy jumps) in the curve, the curve is switched from the figure top to the bottom when given length of time has passed. The parts of the curve enclosed by dotted squares are highly correlated (see Fig. 13)

portion of the original at each shift over the selected time length.

(3) Record the coefficients as a function of time shift. (4) Repeat procedures (1) to (3) until the data are exhausted. Then select the another portion and repeat the procedure (1) to (4). Finally we sort the correlation coefficients to find a maximum value.

An example of the selected portion and the highly correlated portion to that are given in the figure 12 by enclosing them in dotted rectangles. We enlarge and superimpose them on figure 13 and find that Poincare's recurrence theorem (Encyclopedia of Mathematics, 1985) holds approximately in the present system. It is clear that, if we take a shorter portion, we get higher correlation coefficients. If we prepare longer data as an original one, we will get higher values of the coefficient even for the same selected portion. Because the selection of a portion has uncountably many freedom, there may be a more accurately matching portion. These considerations show that the recurrence theorem holds more accurately than shown in figure 13.

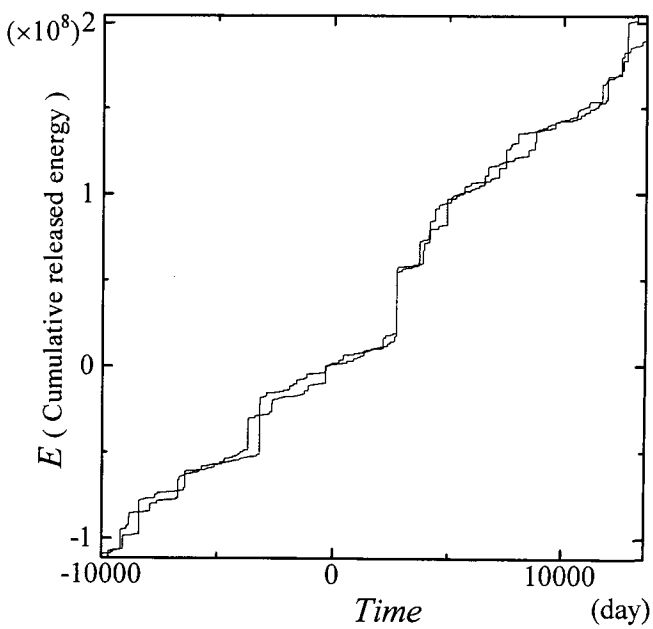

Fig. 13. An example showing ergodic nature of the system. Two curves are enclosed parts of the curve given in Fig. 12. They are in good agreement. This means that the present system satisfies Poincare's recurrence theorem and is approximately ergodic.

(b) Application to real seismic phenomena

Finally we apply our model system to real seismic activities. The data are taken from Seismological bulletin published by Japan meteorological Agency. Selected period is from 1961 to 1995 and five regions are selected and given in figure 14. For each region, the magnitude and time scalings are made according to the magnitude-frequency figure (Fig. 15-X-1) and the return period-frequency figure (Fig. 15-X-2) where X stands for A, . . . , E (in the figures, the return period is denoted as interval time). In figures 15-X-3, cumulation energy curves of the model system (real line) and of the natural seismicity are given.

The calculated curve in each figure is selected from a single common set of data calculated over a very long time period and characteristics of which are given in figures 11 and 12. The procedure for the selection is similar to that stated in the discussion of ergodicity. We select a part of curve of seismic data for the period which begins at 1971/1/1 and ends at 1980/12/31. This ten year part of the curve is shifted along the calculated and scaled curve. Having determined the period of the maximum correlation, we pick up a portion of 20000 days of calculated curve of which center coincide with that of the period of 10 years. In each figure 15-X-3, a short horizontal bar indicates the period

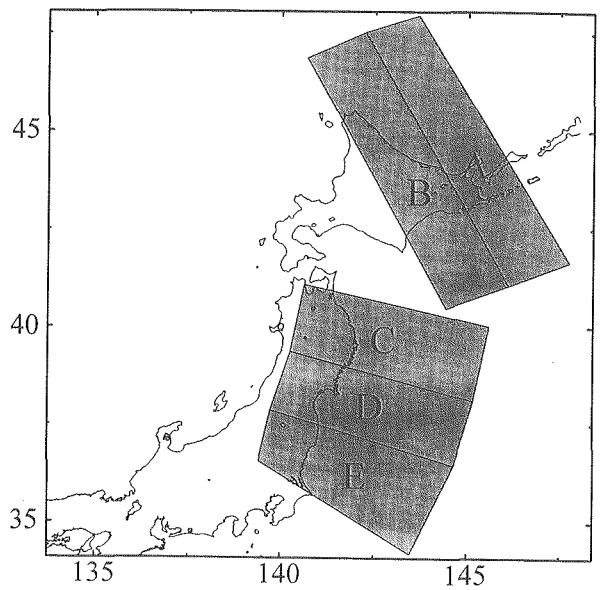

Fig. 14. Seismic activities observed in the regions A, B, . . . , E are compared to the model data.

of 3560 days in which calculated and seismic data are compared.

If the cumulation curve for seismic data outside of the selected period coincides with the calculated one, we can say that our model system well simulates real seismic events. In other words, if the calculated curve well matches with the observed one for later time than the selected period, we can say that the model system predicts a real seismic activity. The reason is that the present model is defined by a system of deterministic differential equations (10). Its nonlinearity causes chaos which may be defined by a phrase "sensitive dependence on initial conditions" (Ruelle, 1979; cited in Drazin, 1992). The short term behavior of the solutions is deterministic. This deterministic nature is completely different from stochastic models consisting of random time series. With these in mind, we examine the figures.

Matching is not sufficiently good for region A but is better for region B, though the magnitude-frequency plots and return period-frequency plots for both regions are similar. For B, timing of steps of calculated curve differs largely from that of the real data (2 to 4 years gap) but the step widths are in good agreement with the real. For region C, agreement between the model and real data is fairly remarkable. This is consistent with the fact that the magnitude-frequency plots and return period-frequency plots have higher quality than the cases of A and B. For regions D and E, agreement is good but seems not so impressive, probably because there is no conspicuous steps in the real data.

The agreement shown by the above examples does not mean that the present model is a physical model of a real system, i.e., earth's crust. Even though we introduced Rayleigh oscillator because of its stick-slip behavior, each unit oscillator in the present model is not considered to represent any real earthquake fault. We should think of the model as a mathematical predictor (nonlinear filter) or one of apparently-physical-but-actually-not-physical models which can well simulate some geophysical phenomena. An example of this kind is the so-called tank model used in hydrology to simulate ground water. Good agreement like case C suggests its prediction ability of seismic activities.

There are at least two possibilities to improve the agreement. We can expect that, if we prepare model data over for a longer time span, we will obtain better agreement. This can easily be done if you use a faster computer (All our calculations were performed on so-called personal computers). The second is to improve the algorithm to judge the correlation. We cannot develop a better algorithm through a logical task but have to resort to empirical methods.

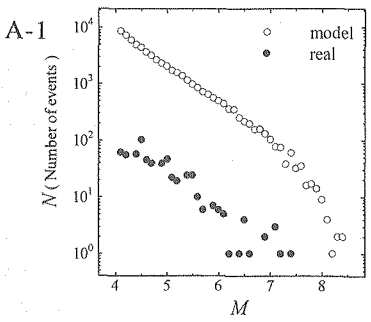
A-1
model
real
N (Number of events)
M

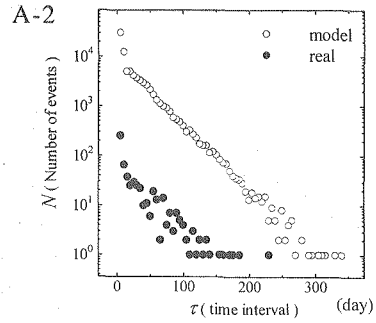
A-2
model
real
N (Number of events)
τ (time interval)
(day)

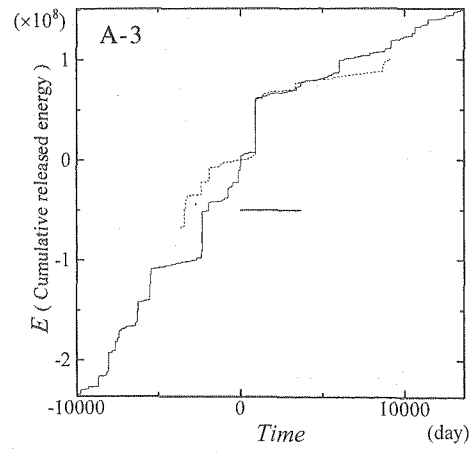
(×10^8)
A-3
E (Cumulative released energy)
Time
(day)

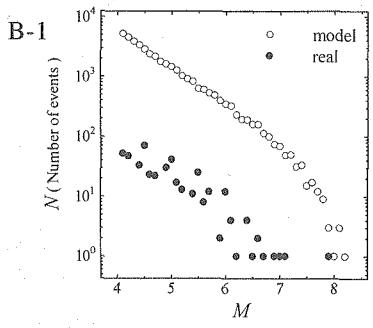
B-1
model
real
N (Number of events)
M

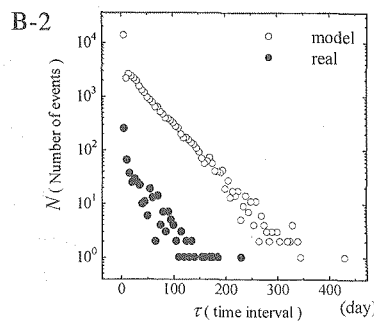
B-2
model
real
N (Number of events)
τ (time interval)
(day)

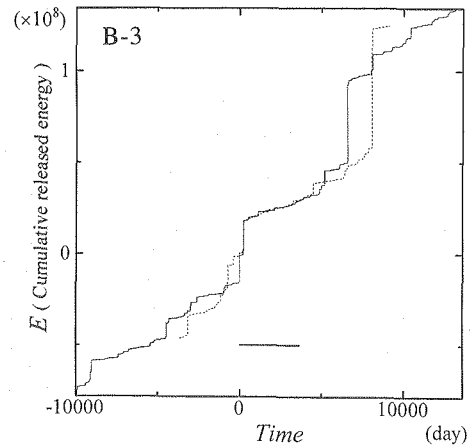
(×10^8)
B-3
E (Cumulative released energy)
Time
(day)

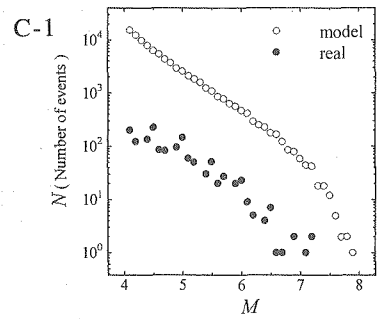
C-1
model
real
N (Number of events)
M

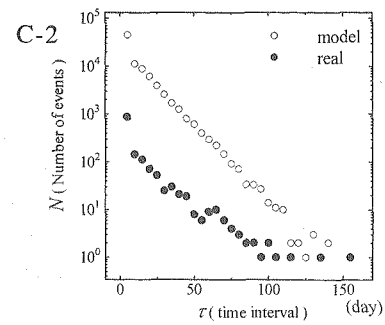
C-2
model
real
N (Number of events)
τ (time interval)
(day)

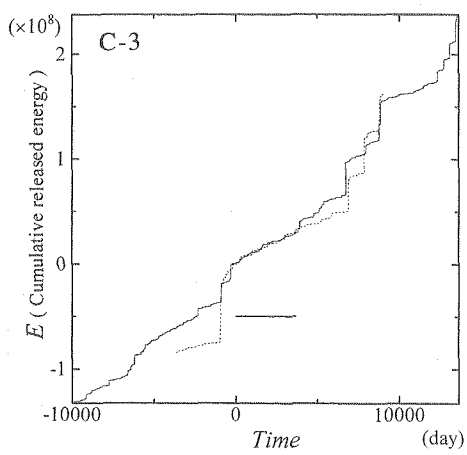
C-3
(×10^8)
E (Cumulative released energy)
Time
(day)

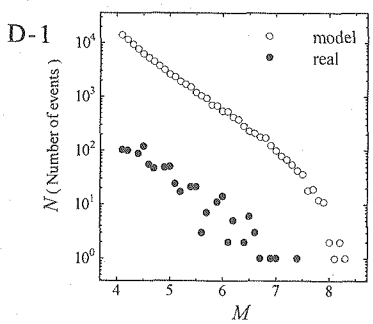
D-1
model
real
N (Number of events)
M

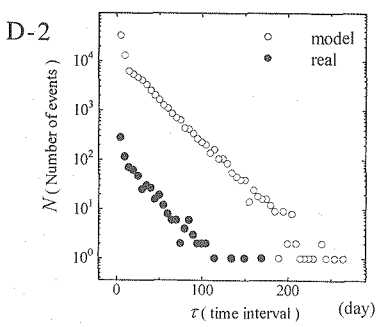
D-2
model
real
N (Number of events)
τ (time interval)
(day)

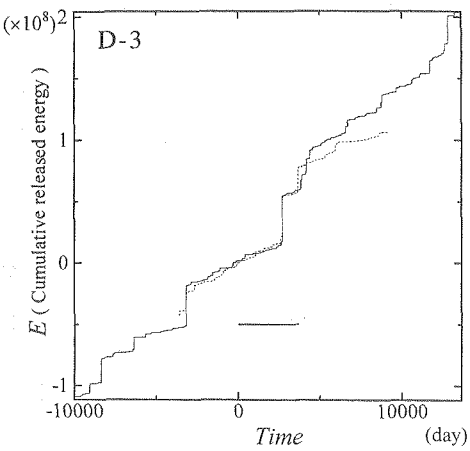
D-3
(×10^8)
E (Cumulative released energy)
Time
(day)

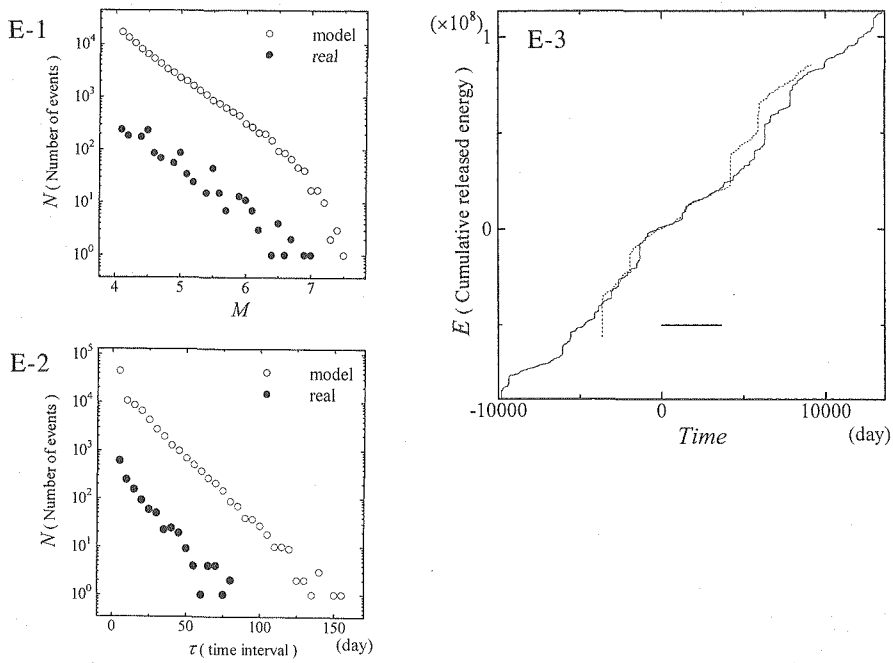

Fig. 15. Magnitude-frequency relations (X-1), return period-frequency relations (X-2) and released energy cumulation curves (X-3) for real seismic data and the model data, where X stands for A, B, . . . , or E. Empty circles in X-1 and X-2 are for the model data and filled circles for real data. In X-3, a dotted curve is for real seismic data and a real curve is a portion selected from the model data given in Fig. 12. The short horizontal bar in the figure X-3 is the period of ten years over which comparison for matching between real and model data was made.

5. Conclusions

We introduced the nonlinear oscillator invented by Rayleigh, which is equivalent to the van der Pol oscillator. We take it as a unit of a system of stick-slip motion. We made a simple and elementary analyses for the single oscillator. The phase portrait shows bifurcation from a limit cycle motion to stable sliding as the driving velocity increases.

Next, we investigated the behavior of the linearly coupled nonlinear oscillators. The bifurcation diagram as a function of driving velocity shows clearly period doubling sequence of bifurcations at several periodic windows within a range of the driving velocity below the bifurcation point of the single oscillator. This means that the system is in a chaotic state for certain range of the

parameter. The diagram also shows strange bifurcation processes. We defined "event" and its "magnitude" for our model system, so that we could compare the model behavior with natural phenomena. The system shows an so-called inverse power law nature for the magnitude-frequency relation.

We constructed a system consisted of multiply and linearly connected Rayleigh oscillators. This system also shows extremely complex bifurcation process for certain range of the driving velocity and also has an inverse power law nature. The law holds for the magnitude-frequency relation and for the return time-frequency relation. The variance of the model data about the relation is reduced as the number of unit oscillators is increased. The ergodic problem on our system was examined numerically. From the energy cumulation curve, we deduced that the Poincare's recurrence theorem held for our model system.

We applied the model to real seismic activities in some regions, Japan, and found that it well simulated these real seismicities. This suggests a possibility to predict seismic activities by the present model which is deterministic for short term behavior.

References

Brace, W.F. and J.D. Byerlee, 1966. Stick-slip as a mechanism for earthquakes, Science, **153**, 990-992.

Burridge, R. and L. Knopoff, 1967. Model and theoretical seismicity, Bull. Seismol. Soc. Am., **57**, 341-371.

Drazin, P.G., 1992. Nonlinear systems, Cambridge.

Mathematical Society of Japan, ed., 1985, Encyclopedia of mathematics, Iwanami.

Rayleigh, J.W.S., 1894. The theory of sound, Macmillan (reprint Dover, 1945).

Ruelle, D., 1979. Sensitive dependence on initial conditions and turbulent behavior of dynamical systems., Ann. N.Y. Acad. Sci., **316**, 408-416.

Strogatz, S.H., 1994. Nonlinear dynamics and chaos, Addison Wesley.

Yokomori, M., 1997. Dynamic model of a fault using coupled Rayleigh's oscillators, Master's thesis, Graduate School of Science (Geophysics), Hokkaido University (in Japanese).

Utsu, T., 1977. Seismology, Kyouritu (in Japanese).